The Bcl-2 homolog Nrz inhibits binding of IP3 to its receptor to control calcium signaling during zebrafish epiboly

Benjamin Bonneau, Adrien Nougarède, Julien Prudent, Nikolay Popgeorgiev, Nadine Peyriéras, Ruth Rimokh, Germain Gillet

The Bcl-2 Homolog Nrz Inhibits Binding of IP_3 to Its Receptor to Control Calcium Signaling During Zebrafish Epiboly

Benjamin Bonneau,[1] Adrien Nougarède,[1] Julien Prudent,[1] Nikolay Popgeorgiev,[1] Nadine Peyriéras,[2] Ruth Rimokh,[1] Germain Gillet[1]*

Members of the Bcl-2 protein family regulate mitochondrial membrane permeability and also localize to the endoplasmic reticulum where they control Ca^{2+} homeostasis by interacting with inositol 1,4,5-trisphosphate (IP_3) receptors (IP_3Rs). In zebrafish, Bcl-2–like 10 (Nrz) is required for Ca^{2+} signaling during epiboly and gastrulation. We characterized the mechanism by which Nrz controls IP_3-mediated Ca^{2+} release during this process. We showed that Nrz was phosphorylated during early epiboly, and that in embryos in which Nrz was knocked down, reconstitution with Nrz bearing mutations designed to prevent its phosphorylation disrupted cyclic Ca^{2+} transients and the assembly of the actin-myosin ring and led to epiboly arrest. In cultured cells, wild-type Nrz, but not Nrz with phosphomimetic muta-tions, interacted with the IP_3 binding domain of IP_3R1, inhibited binding of IP_3 to IP_3R1, and prevented histamine-induced increases in cytosolic Ca^{2+}. Collectively, these data suggest that Nrz phosphorylation is necessary for the generation of IP_3-mediated Ca^{2+} transients and the formation of circumferential actin-myosin cables required for epiboly. Thus, in addition to their role in apoptosis, by tightly regulating Ca^{2+} signaling, Bcl-2 family members participate in the cellular events associated with early vertebrate devel-opment, including cytoskeletal dynamics and cell movement.

INTRODUCTION

The Bcl-2 protein family has both pro- and antiapoptotic functions, including the control of mitochondrial membrane permeability to cytochrome c, which leads to caspase activation (*1*). In addition, Bcl-2 proteins localize to the endoplasmic reticulum (ER) where they participate in Ca^{2+} homeostasis by binding to the Ca^{2+} channel, inositol 1,4,5-trisphosphate (IP_3) receptor (IP_3R) (*2*). IP_3 binding to IP_3Rs promotes Ca^{2+} efflux from the ER into the cytosol, a process known as IP_3-induced Ca^{2+} release (IICR). IP_3Rs are composed of five types of domains (*3*): the suppressor domain (SD), the IP_3-binding domain (IP_3BD), the modulatory and transducing domain (MTD), the channel-forming domain (CFD), and the coupling domain (CD). The SD and IP_3BD mediate binding to IP_3, the MTD binds regulatory molecules that modify IP_3R activity and transduces the signal from the IP_3BD to the CFD, and the CD is implicated in IP_3R tetramerization and channel opening (*4*). Bcl-2 inhibits IICR by interacting with the MTD (*5*), whereas Bcl-xL promotes Ca^{2+} release at low concentrations of IP_3 by interacting with the CD (*6*).

Ca^{2+} release through IP_3Rs mediates many cellular and physiological processes, such as cell proliferation, differentiation, apoptosis, fertilization, and embryonic development (*7*). In the zebrafish embryo, Ca^{2+} signaling plays a role in early stages of development (*8*). At the onset of the blastula stage, blastomeres that are in contact with the yolk release the contents of their cytoplasm into the yolk cell forming the yolk syncytial layer (YSL). At the end of blastulation, the embryo comprises blastomeres on top of the yolk cell, which contains the YSL. Before gastrulation, the blastomeres and the YSL begin to migrate from the animal to the vegetal pole in a process known as epiboly (*9*). In the YSL, IP_3R-dependent Ca^{2+} signaling occurs at the onset of epiboly (*10*) and again once the blastomeres have passed the equator of the embryo (*11*). A contractile actin-myosin ring forms at the blastoderm margin (*12*) and is likely required for epiboly progression.

We recently demonstrated that the antiapoptotic protein Nrz, the zebrafish ortholog of Nrh-Bcl2l10, plays a crucial role in the progression of zebrafish epiboly. During early development, zygotic *nrz* is specifically expressed in the YSL, and knockdown of Nrz by morpholino (MO) injection results in epiboly arrest, constriction of the blastoderm margin, and detachment of the embryo from the yolk cell (*13*). This phenotype does not require caspase activity; instead, Nrz binds to IP_3R1 on the surface of the ER and decreases IICR (*14*). Knockdown of *nrz* increases the concentration of Ca^{2+} at the blastoderm margin and promotes phosphorylation of myosin light chain (MLC) and premature formation of the circumferential actin-myosin ring, resulting in the detachment of blastomeres from the yolk (*14*).

Here, we investigated how Nrz regulates Ca^{2+} signals in the YSL during epiboly. We demonstrated that Nrz interacted with the IP_3BD of IP_3R1 and disrupted its binding to IP_3. Furthermore, we showed that phosphorylation of Nrz prevented this interaction and promoted Ca^{2+} oscillations and formation of the actin-myosin ring during epiboly.

RESULTS

The BH4-BH1 region of Nrz is required to inhibit IICR

We previously demonstrated that Nrz interacts with IP_3R1 via its N-terminal Bcl-2 homology (BH) 4 domain (*14*). Other members of the Bcl-2 family, including Bcl-2 and Bcl-xL, interact with IP_3R1 (*5*, *6*) and control IICR. Although the BH4 domain of Bcl-2 is sufficient to suppress IICR (*15*), the BH4 domain of Bcl-xL is not (*16*). To determine whether the BH4 domain of Nrz was required for IICR inhibition, we fused the BH4 domain of Nrz to the ER-targeting sequence of cytochrome b5 (NrzBH4Cb5) (Fig. 1A)

[1]Université de Lyon, Centre de recherche en cancérologie de Lyon, U1052 INSERM, UMR CNRS 5286, Université Lyon I, Centre Léon Bérard, 28 rue Laennec, 69008 Lyon, France. [2]CNRS-MDAM, UPR 3294 and BioEmergences-IBiSA, Institut de Neurobiologie Alfred Fessard, Avenue de la Terrasse, 91198 Gif-sur-Yvette Cedex, France.
*Corresponding author. E-mail: germain.gillet@univ-lyon1.fr

and transiently overexpressed the fusion protein in HeLa cells. Similar to the Nrz BH4 domain that localizes in the cytoplasm (*14*) or full-length Nrz targeted to the ER (NrzCb5), NrzBH4Cb5 coimmunoprecipitated with endogenous IP_3R1 (Fig. 1B). To assess whether NrzBH4Cb5 affects IICR, we monitored changes in the concentration of cytosolic Ca^{2+} using a Ca^{2+}-sensitive fluorescent dye. In human umbilical vein endothelial cells, histamine triggers IP_3 accumulation and increases cytosolic Ca^{2+}, which can be reversed by inhibition of protein kinase C (*17*). We found that treating HeLa cells with histamine induced a transient increase in the concentration of cytosolic Ca^{2+} and that overexpression of NrzCb5, but not of NrzBH4Cb5, partially inhibited this effect (Fig. 1, C and D), suggesting that the BH4 domain is not sufficient to inhibit IICR.

Nrz contains a total of four BH domains, numbered BH4, BH3, BH1, and BH2, from the N to the C terminus (Fig. 1A). Thus, we asked whether longer N-terminal fragments of Nrz containing other BH domains could affect IICR. Consistent with the fact that the BH4 domain of Nrz mediates its interaction with IP_3R1, we found that all forms of C-terminally truncated Nrz coimmunoprecipitated with endogenous IP_3R1 (Fig. 1E). However, overexpression of the Nrz BH1, BH3, and BH4 domains (Nrz1-94Cb5) significantly reduced histamine-induced increased cytosolic Ca^{2+}, whereas overexpression of the Nrz BH3 and BH4 domains (Nrz1-67Cb5) did not (Fig. 1, F and G), suggesting that the BH1 domain is required for IICR.

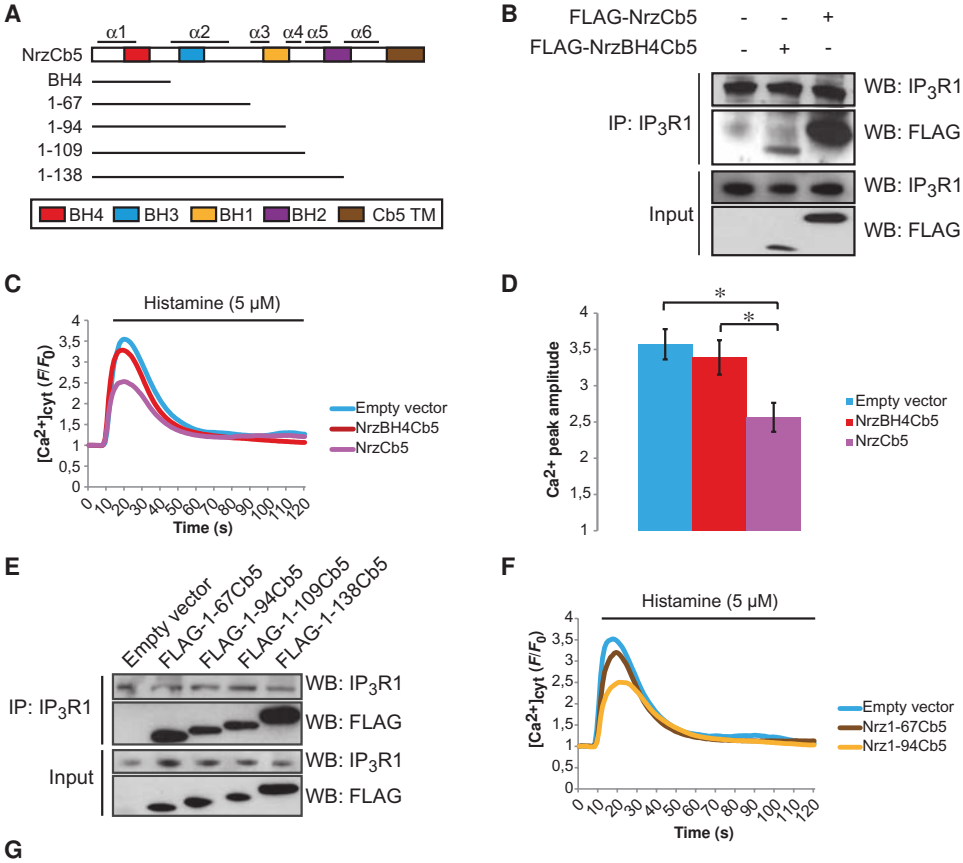

Fig. 1. Nrz requires its BH4-BH1 region to bind IP_3R1 and regulate IICR in HeLa cells. (A) Schematic of full-length Nrz and the Cb5 domain of cytochrome b. Lines and colored boxes represent α helices and BH domains, respectively. (B) Representative Western blot of immunoprecipitation (IP) between endogenous IP_3R1 and FLAG-NrzBH4 or FLAG-NrzCb5. $n = 3$. (C) Representative Ca^{2+} response curve of cells stimulated with 5 μM histamine at the indicated times. Cells were transfected with empty vector, FLAG-NrzBH4Cb5, or FLAG-NrzCb5. (D) Histogram showing the mean amplitude (±SD) of the histamine-induced Ca^{2+} peak. $n \geq 5$ fields from biological replicates. (E) Representative Western blot of IP between endogenous IP_3R1 and FLAG-tagged C-terminal Nrz deletion mutants. $n = 3$. (F) Representative Ca^{2+} response curve of cells stimulated with 5 μM histamine at the indicated times. Cells were transfected with empty vector, FLAG-Nrz1-67Cb5, or FLAG-Nrz1-94Cb5. (G) Histogram showing the mean amplitude (±SD) of the histamine-induced Ca^{2+} peak. $n \geq 5$ fields from biological replicates. *$P < 0.005$ (Mann-Whitney *U* test) for (D) and (G).

Nrz inhibition of IICR is independent of its interaction with the proapoptotic protein Bax

The fact that the BH1 domain of Nrz was required for its interaction with IP_3R1 could mean that the ability of Nrz to inhibit IICR is related to its ability to bind proapoptotic members of the Bcl-2 family. The BH1 domain of Bcl-2 family proteins contains a conserved Asn-Try-Gly-Arg motif. Mutation of Gly^{145} to Ala in Bcl-2 prevents its heterodimerization with the proapoptotic protein Bax (*18*). To test whether the analogous residue in Nrz mediated dimerization with Bax, we mutated Gly^{85} to Ala in otherwise wild-type Nrz (NrzG85A). We found that full-length wild-type Nrz, but not NrzG85A or Nrz1-94, coimmunoprecipitated endogenous Bax (Fig. 2A) and reduced the abundance of cleaved poly (adenosine 5′-diphosphate–ribose) polymerase (PARP) induced by overexpression of Bax in HeLa cells (Fig. 2B), suggesting that the Gly^{85} residue in the BH1 domain is important for Nrz-dependent inhibition of Bax-mediated apoptosis. Thus, we asked whether Gly^{85} was required for Nrz to inhibit IICR. We fused the NrzG85A to the ER-targeting Cb5 domain (NrzG85ACb5) and expressed it in HeLa cells. We found that NrzG85ACb5 significantly reduced histamine-induced increases in cytosolic Ca^{2+} (Fig. 2, C and D). Collectively, these results suggest that the function of Nrz to inhibit IICR is most likely independent of binding to Bax.

Nrz binds to the IP_3BD of zIP_3R1

The BH4 domain of several antiapoptotic Bcl-2 family proteins, including Bcl-2 and Bcl-xL, interacts with either the MTD or CD of IP_3R1, which is determined by the primary sequence of the BH4 domains (*5*, *6*, *16*, *19*, *20*). The primary sequence of the Nrz BH4 domain differs considerably from those of zBcl-2 and zBcl-xL (fig.

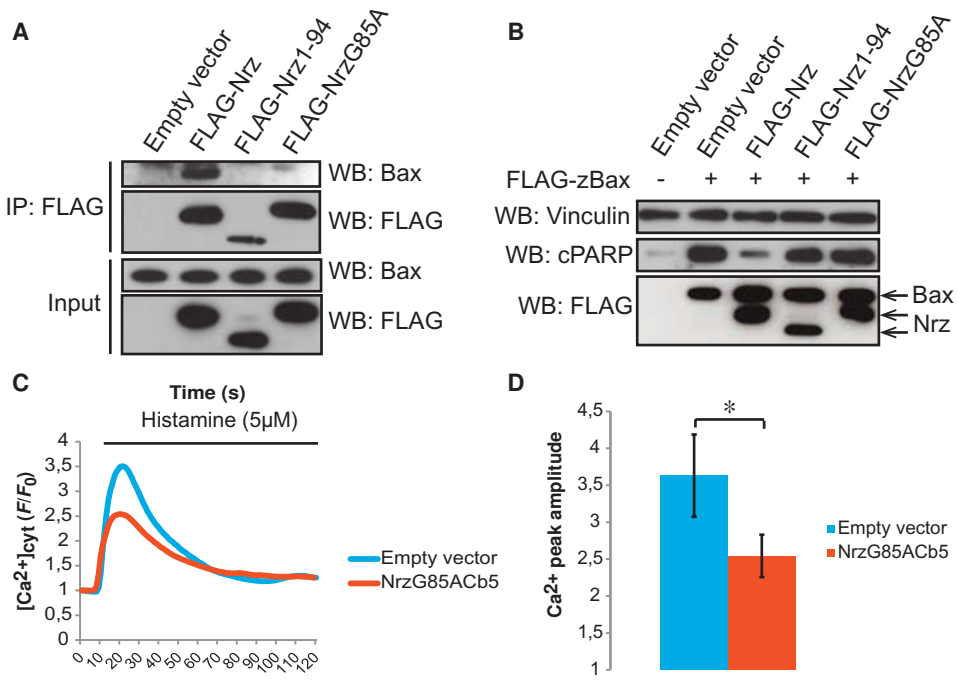

Fig. 2. Nrz regulates IICR in HeLa cells independent of its interaction with Bax. (**A**) Representative Western blot of IP between endogenous Bax and FLAG-tagged Nrz, Nrz1-94, or NrzG85A. $n = 3$. (**B**) Representative Western blot of cleaved PARP (cPARP) in cells transiently expressing zBax (zebrafish Bax) and FLAG-tagged full-length Nrz, Nrz1-94, or NrzG85A. $n = 3$. (**C**) Representative Ca^{2+} response curve of cells stimulated with 5 μM histamine at the indicated times. Cells were transfected with empty vector or FLAG-NrzG85ACb5. (**D**) Histogram showing mean amplitude (±SD) of the histamine-induced Ca^{2+} peak. $n \geq 5$ fields from biological replicates. $^*P < 0.005$ (Mann-Whitney *U* test).

S1). To determine which domain of Nrz interacts with IP_3R1, we expressed fragments of zebrafish IP_3R1 (zIP_3R1) (Fig. 3A) in HeLa cells. We found that the IP_3BD, but not the SD, MTDs, or CD, of zIP_3R1 coimmunoprecipitated NrzCb5 (Fig. 3B) but not NrzCb5 lacking the BH4 domain (NrzΔBH4Cb5) (fig. S2), suggesting that the interaction between Nrz and IP_3R1 is mediated by the specific binding of the IP_3BD of IP_3R1 to the BH4 domain of Nrz.

Nrz binds outside the IP_3 binding pocket of IP_3R1

A group of residues in the IP_3BD form a positively charged pocket in the IP_3-binding site (*21*). In mouse IP_3R1, point mutations in these residues abolish the binding of both IP_3 (*21*) and IRBIT (IP_3R-binding protein released with IP_3), a competitive inhibitor of IP_3 (*22*, *23*). These residues are conserved in zebrafish; therefore, we asked whether they were required for binding to Nrz. Individual mutations to each of the corresponding amino acids did not affect the ability of the IP_3BD of zIP_3R1 to coimmunoprecipitate NrzCb5 (Fig. 3C) when coexpressed in HeLa cells, suggesting that, unlike IRBIT, Nrz does not act as a competitive inhibitor of IP_3 binding to IP_3R1.

To identify which residues could govern the interaction of IP_3R1 and Nrz, we performed molecular docking simulation between the IP_3BD of mouse IP_3R1 [Protein Data Bank (PDB): 1N4K] and the BH4 domain of Nrz (Fig. 3D). This analysis suggested that Nrz interacts with IP_3R1 outside of the IP_3 binding pocket, consistent with the mutational analysis (Fig. 3C), and identified three residues in IP_3R1 that could mediate its interaction with Nrz. We mutated the corresponding residues in zIP_3R1 (Glu^{255}, Glu^{410}, and Tyr^{576}) and performed coimmunoprecipitation experiments in HeLa cells. We found that E225A prevented the interaction of NrzCb5 with the IP_3BD (Fig. 3E), indicating that Glu^{255} of zIP_3R1 was critical for binding to Nrz. Analysis of docking solutions also indicated that the interaction of Nrz and IP_3R1 may depend on the interaction between zIP_3R1 Glu^{255} and Cys^{20} of Nrz. Analysis of primary sequence alignments demonstrated that Cys^{20} is highly conserved across Nrz orthologs (fig. S3), suggesting that this residue could be important for binding between Nrz and zIP_3R1 and that this interaction could be evolutionarily conserved.

Nrz prevents IP_3 from binding to IP_3R1

We found that Nrz inhibits IICR and binds to the IP_3BD of IP_3R1, suggesting that it could interfere with IP_3 binding to IP_3R1. We verified that Nrz does not affect the steady-state concentration of Ca^{2+} in the ER. In HeLa cells, expression of NrzCb5 did not affect increased cytosolic Ca^{2+} caused by treatment with thapsigargin (fig. S4), which inhibits the sarco-endoplasmic reticulum Ca^{2+} adenosine triphosphatase (ATPase) and thereby flushes Ca^{2+} from the ER (*24*).

To test whether Nrz could prevent binding of IP_3 to IP_3R1 to inhibit IICR, we used the IP_3R-based IP_3 sensor (IRIS), which contains the IP_3BD flanked by enhanced cyan fluorescent protein (ECFP) and the yellow fluorescent protein Venus. When IP_3 binds to IRIS, it induces a conformational change in the IP_3BD that decreases fluorescence resonance energy transfer (FRET) from ECFP to Venus (*25*). Treating HeLa cells expressing IRIS with histamine induced a rapid increase in the ratio (*R*) between ECFP and Venus fluorescence intensities, indicating reduced FRET (Fig. 4A). Transient overexpression of full-length wild-type Nrz or Nrz1-94, but not NrzBH4 or NrzΔBH4, prevented histamine-induced changes in the IRIS FRET ratio (Fig. 4, A and B). We also directly assessed the binding of IP_3 to IP_3R1 using fluorescence polarization (*26*) to measure the interaction between IP_3 covalently bound to fluorescein isothiocyanate (IP_3-FITC) and a recombinant protein composed of the SD and IP_3BD of IP_3R1 (IP_3R1-NTD). When we incubated IP_3-FITC with IP_3R1-NTD in the presence of recombinant Nrz, we found that Nrz reduced fluorescence polarization in a concentration-dependent manner (half-maximal inhibitory concentration, $2.96 \times 10^{-8} \pm 1.77 \times 10^{-8}$ M) (Fig. 3C). Collectively, these results demonstrate that Nrz inhibits the binding of IP_3 to IP_3R1.

Phosphorylation of Nrz inhibits its interaction with IP_3R1

We hypothesized that the interaction between endogenous Nrz and IP_3R1 could be regulated by signal transduction mechanisms such as phosphorylation. Phosphorylation of Bcl-2 on a Thr and two Ser residues in the loop between its BH4 and BH3 domains increases Ca^{2+} release from the ER (*27*). Similar to Bcl-2, Nrz has a Thr and two Ser residues in the loop between the BH4 and BH3 domains (Fig. 5A) that could be phosphorylated. We mutated these three residues to generate phosphomimetic (T26D, S29D, S31D, NrzDDD) and nonphosphorylatable (T26A, S29A, S31A,

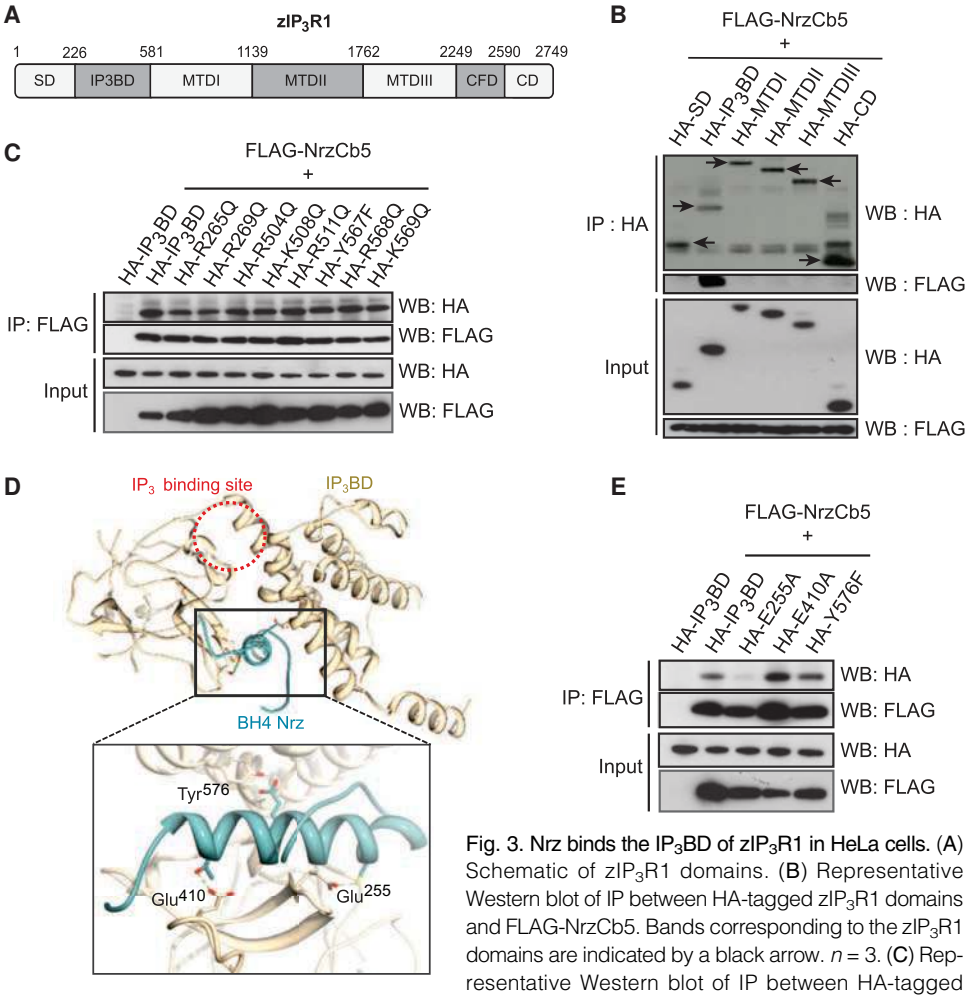

Fig. 3. Nrz binds the IP_3BD of zIP_3R1 in HeLa cells. (**A**) Schematic of zIP_3R1 domains. (**B**) Representative Western blot of IP between HA-tagged zIP_3R1 domains and FLAG-NrzCb5. Bands corresponding to the zIP_3R1 domains are indicated by a black arrow. $n = 3$. (**C**) Representative Western blot of IP between HA-tagged IP_3BD or IP_3BD binding site mutants and FLAG-NrzCb5. $n = 3$. (**D**) Docking model of the BH4 domain of Nrz (modeled by multi-template homology with Phyre[2]) binding to the IP_3BD of mouse IP_3R1 (PDB: 1N4K). The red dashed circle represents the IP_3 binding site. (**E**) Representative Western blot of IP between HA-tagged IP_3BD domain or IP_3BD mutants (E255A, E410A, Y576F) and FLAG-NrzCb5. $n = 3$.

NrzAAA) amino acid versions of Nrz. When transiently expressed in HeLa cells, NrzAAACb5, but not NrzDDDCb5, significantly decreased histamine-induced increased cytosolic Ca^{2+} (Fig. 5, B and C). Moreover, NrzAAACb5, but not NrzDDDCb5, coimmunoprecipitated the IP_3BD of IP_3R1 (Fig. 5D). To identify which of these three amino acids was important for Nrz interaction with IP_3R1, we generated single and double mutants at each position. We found that Nrz mutants containing S31D did not coimmunoprecipitate the IP_3BD of IP_3R1 (Fig. 5E), suggesting that Ser^{31} phosphorylation by an unknown kinase could play a critical role in inhibiting the interaction between Nrz and IP_3R1 and promoting IICR.

Domains of Nrz required for the inhibition of IICR are also required for zebrafish epiboly

We previously reported that Nrz knockdown by antisense MO injection results in the constriction of the blastoderm margin and the detachment of the embryo from the yolk cell during epiboly (*13*). The injection of *nrz* MO induces a robust increase in cytosolic Ca^{2+} and embryonic lethality, which can be prevented by co-injecting mRNA encoding NrzCb5 but not NrzΔBH4Cb5 (*14*). Here, we found that both the BH4 and BH1 domains of Nrz were required to inhibit IICR in HeLa cells (Fig. 1). Therefore, we tested whether these domains were sufficient to reverse the phenotype induced by *nrz* MO injection. We co-injected embryos with *nrz* MO and in vitro–synthesized mRNA encoding various truncated forms of Nrz and monitored the percentage of embryos showing abnormal margin constriction during epiboly (Fig. 6A). Co-injection of *nrzbh4cb5* did not prevent epiboly defects induced by *nrz* MO (Fig. 6, A and B), consistent with the observation that the BH4 domain was not sufficient to reduce IICR in HeLa cells. Moreover, co-injection of *nrz1-94cb5*, but not of *nrz1-67cb5*, also prevented epiboly defects induced by *nrz* MO (Fig. 6C), demonstrating a requirement for the BH1 domain of Nrz in this process. We also found that the ability of Nrz to prevent IICR was independent of its ability to bind to Bax in HeLa cells (Fig. 2C). Similarly, co-injection of *nrzG85A*, which encodes a form of Nrz that does not bind Bax (Fig. 2A), prevented epiboly defects induced by *nrz* MO (Fig. 6D). Finally, we found that Nrz phosphorylation could impair its interaction with IP_3R1 in HeLa cells (Fig. 5D). In zebrafish, co-injection of *nrz* MO with *nrzAAAcb5*, but not *nrzDDDcb5*, reduced the percentage of embryos with epiboly defects induced by *nrz* MO (Fig. 6E). Thus, the domains and residues of Nrz required to inhibit IICR in cultured cells are also required for zebrafish epiboly.

Phosphorylation of Nrz enables Ca^{2+} signaling, actin-myosin ring formation, and epiboly

During epiboly, IP_3-dependent cyclic increases in cytosolic Ca^{2+} concentration, referred to as Ca^{2+} waves, occur in the YSL (*10*), where *nrz* is expressed (*13*). Because Nrz inhibits IP_3 binding to IP_3R1 in HeLa cells (Fig. 4, A to C), we hypothesized that Nrz activity is negatively regulated to enable the generation of Ca^{2+} waves. In HeLa cells, we found that mutants of Nrz that mimic phosphorylated Thr and Ser do not bind to IP_3R1 (Fig. 5D) or inhibit IICR (Fig. 5C). To examine whether Nrz is phosphorylated during epiboly in vivo, we injected *nrzcb5* mRNA and immunoprecipitated NrzCb5 from ER fractions prepared from the YSL of embryos at different developmental stages. Western blot analysis revealed that Nrz Ser phosphorylation was barely detectable before the onset of epiboly and increased robustly by 30% epiboly (Fig. 7A), suggesting that Nrz phosphorylation could be important to enable IP_3-dependent Ca^{2+} signaling in vivo during this process.

We tested whether replacing endogenous Nrz with a nonphosphorylatable form of Nrz could disrupt Ca^{2+} signaling. In wild-type embryos injected at the 128-cell stage with a Ca^{2+}-sensitive dye, we observed cyclic Ca^{2+} waves in the YSL at 30% epiboly (Fig. 7, B to E, and movie S1). To evaluate the contribution of Nrz phosphorylation to the generation of these Ca^{2+} waves, we co-injected *nrz* MO and *nrzAAAcb5* or *nrzcb5*. We found that *nrzcb5*, but not *nrzAAAcb5*, restored normal Ca^{2+} waves in the absence of endogenous

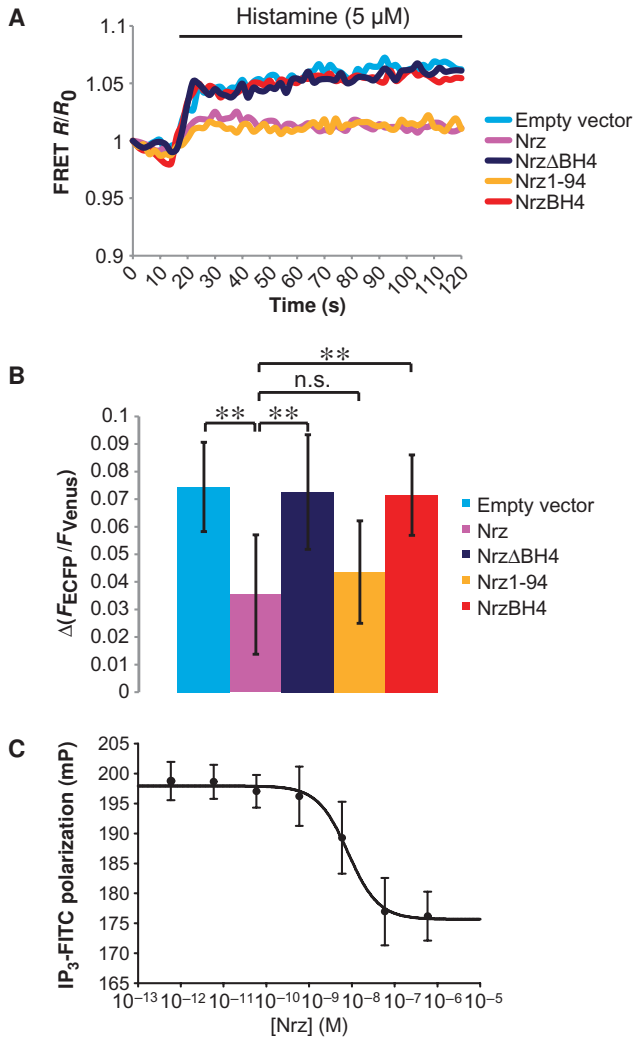

Fig. 4. Nrz prevents IP_3 binding to IP_3R1. (**A**) Representative curve of the FRET signal change of IRIS in HeLa cells stimulated with 5 μM histamine and expressing the indicated proteins. The FRET signal was calculated as the ratio (*R*) of fluorescence emission of ECFP to fluorescence emission of Venus with excitation at 405 nm. (**B**) Histogram showing the mean FRET signal change (±SD) induced by histamine stimulation. *n* = 30 cells from at least 3 biological replicates. $^{**}P < 0.0001$ (Mann-Whitney *U* test); n.s., nonsignificant ($P > 0.1$). (**C**) Curve showing the mean fluorescence polarization (±SD) of IP_3-FITC in the presence of IP_3R1 NTD and the indicated concentration of recombinant Nrz protein. *n* = 3 independent triplicate measurements.

Nrz (Fig. 7, B to E, and movies S2 and S3), suggesting that the phosphorylation of Nrz enables the generation of YSL Ca^{2+} waves at the beginning of epiboly.

An actin-myosin ring forms at the blastoderm margin in zebrafish embryos at 40% epiboly, and localized disruption of actin in the YSL at 60% epiboly delays cell movements associated with epiboly progression (*12*). Similarly, treating zebrafish embryos at 50% epiboly with cytochalasin B, which inhibits actin network formation, or with a Ca^{2+} chelator disrupts actin ring formation and epiboly (*28*), suggesting that Ca^{2+} waves are important for the formation of the actin-myosin ring. Given that *nrzAAAcb5* disrupted Ca^{2+} waves when co-injected with *nrz* MO, we examined the formation of the actin-myosin ring. Co-injection of *nrz* MO with *nrzAAAcb5*, but not *nrzcb5* or *nrz* MO injection alone, reduced F-actin staining at the blastoderm margin at 50% epiboly (Fig. 8, A and B), suggesting that the expression of nonphosphorylatable Nrz inhibits YSL Ca^{2+} dynamics and thereby disrupts the formation of the actin-myosin ring.

The above data suggested that the phosphorylation of Nrz could be important for epiboly progression. In embryos injected with *nrz* MO, co-injection of *nrzAAAcb5*, but not of *nrzcb5*, resulted in epiboly delay (Fig. 8C) or arrest (Fig. 8D). Collectively, these results suggest that by 50% epiboly, endogenous Nrz is mostly phosphorylated and cannot bind to IP_3R1 and is thus permissive to Ca^{2+} signaling required for actin assembly and contractility.

DISCUSSION

We found that Nrz binds outside the IP_3 binding site on the IP_3BD of IP_3R1 and prevents IP_3 binding, revealing a new regulatory mechanism for IP_3Rs by Bcl-2–related proteins. Bcl-2 reduces Ca^{2+} release by interacting with the MTD of IP_3R1 (*5*, *15*), and Bcl-xL sensitizes IP_3R1 to low IP_3 concentrations by interacting with the CD (*6*). The differential binding of Bcl-2 proteins to various domains of IP_3R1 may be determined by divergent amino acid sequences in the BH4 domains (*16*, *20*). Here, we found that the BH4 domain of Nrz was sufficient for it to interact with IP_3R1, suggesting that residues within this domain could be critical for determining the interaction with the IP_3BD. Molecular docking simulation identified a conserved Cys (Cys^{20} in Nrz) as a potential factor in mitigating the binding of Nrz to the IP_3BD of IP_3R1. We found that Glu^{255} of zIP_3R1 most likely contacts Nrz Cys^{20} and is essential for binding between these proteins. Whether Nrz Cys^{20} is required to bind IP_3R1 and whether analogous residues confer specificity of binding of Bcl-2 family and other proteins to IP_3BDs remain to be determined.

Several proteins interact with the IP_3BD or decrease IP_3 binding to the IP_3R1. Beclin-1 binds to the IP_3BD of IP_3R1, but Beclin-1 knockdown has no effect on Ca^{2+} homeostasis (*29*). Sodium-potassium ATPase binds to the IP_3BD of IP_3R1 (*30*) and promotes Ca^{2+} release in the absence IP_3 (*31*). Carbonic anhydrase–related protein (CARP) inhibits IP_3 binding to IP_3R1 by reducing the affinity of the receptor for IP_3 (*32*). CARP interacts with the MTD of IP_3R1 (*32*), suggesting that Nrz and CARP act by distinct mechanisms. IRBIT binds the IP_3BD of IP_3R1 and directly competes with IP_3 for binding to its receptor (*22*, *23*). We found that mutations in residues of IP_3R1 required for interaction with IRBIT and IP_3 were not required for binding to Nrz, suggesting that Nrz and IRBIT act by distinct mechanisms to inhibit IP_3R1. The Nrz BH4 domain binds outside the IP_3 binding site of IP_3R1, and the inhibition of IICR by Nrz requires the 94 most N-terminal amino acids including the BH4, BH3, and BH1 domains. The BH4 and BH3 domains combined were not sufficient to inhibit IICR without the BH1 domain, despite still being able to bind to IP_3R1. These findings imply that Nrz is an allosteric inhibitor. Binding of Nrz could produce a conformational change in the IP_3BD of IP_3R1 that decreases the affinity of the IP_3 binding site for IP_3. Alternatively, Nrz, potentially involving its BH1 domain, could hinder access of IP_3 to the IP_3 binding site on IP_3R1 without direct competition for key residues.

The mutation of putative phosphorylated residues to phosphomimetic amino acids in Nrz prevented its ability to inhibit IICR and bind IP_3R1. Mutation of analogous residues in Bcl-2 to nonphosphorylatable amino acids enhances its ability to reduce Ca^{2+} release from the ER (*27*). However, this effect is indirect. Phosphorylation of Bcl-2 reduces its interactions with proapoptotic proteins, such as Bax, which increases ER Ca^{2+} content by reducing the Ca^{2+} leak (*33*). Nrz did not alter basal ER Ca^{2+}

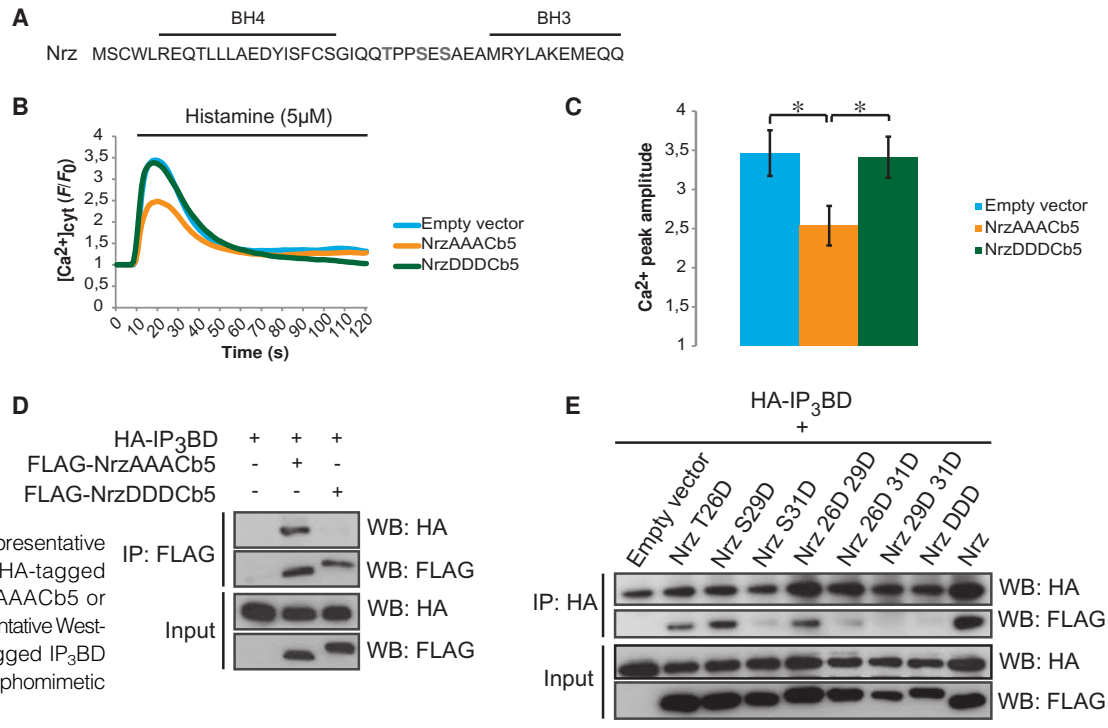

Fig. 5. Phosphomimetic mutant Nrz does not bind IP_3R1 or inhibit IICR in HeLa cells. (A) Primary sequence of the Nrz protein including the BH4 and BH3 domains. Putative phospho-serines and phospho-threonine are shown in red. (B) Representative Ca^{2+} response curve of cells stimulated with 5 µM histamine at the indicated times. Cells were transfected with empty vector, FLAG-NrzAAACb5, or FLAG-NrzDDDCb5. (C) Histogram showing the mean amplitude (±SD) of the histamine-induced Ca^{2+} peak. $n \geq 5$ fields from biological replicates. $^*P < 0.005$ (Mann-Whitney U test). (D) Representative Western blot of IP between HA-tagged IP_3BD and FLAG-tagged NrzAAACb5 or NrzDDDCb5. $n = 3$. (E) Representative Western blot of IP between HA-tagged IP_3BD and FLAG-tagged Nrz or phosphomimetic Nrz mutants.

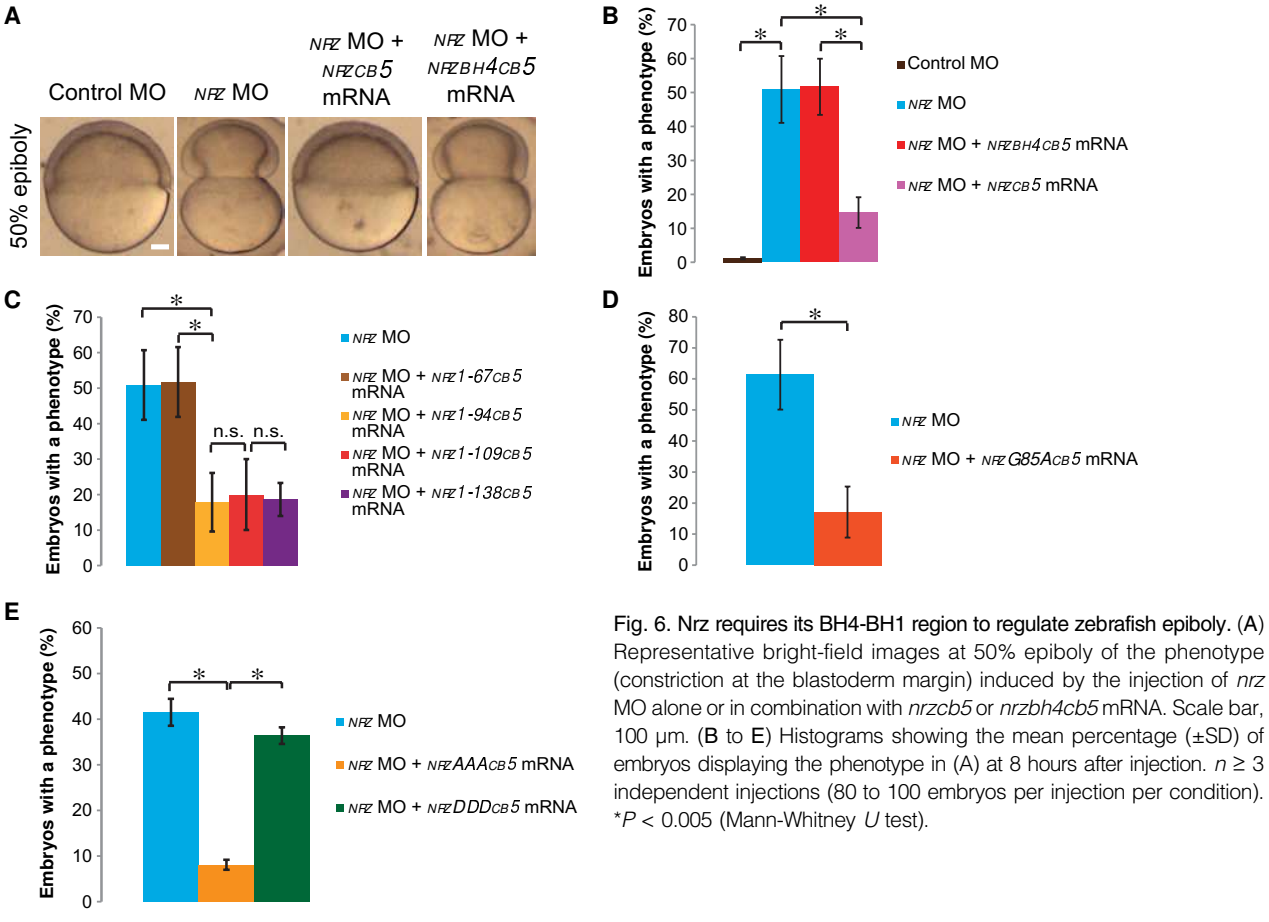

Fig. 6. Nrz requires its BH4-BH1 region to regulate zebrafish epiboly. (A) Representative bright-field images at 50% epiboly of the phenotype (constriction at the blastoderm margin) induced by the injection of *nrz* MO alone or in combination with *nrzcb5* or *nrzbh4cb5* mRNA. Scale bar, 100 µm. (B to E) Histograms showing the mean percentage (±SD) of embryos displaying the phenotype in (A) at 8 hours after injection. $n \geq 3$ independent injections (80 to 100 embryos per injection per condition). $^*P < 0.005$ (Mann-Whitney U test).

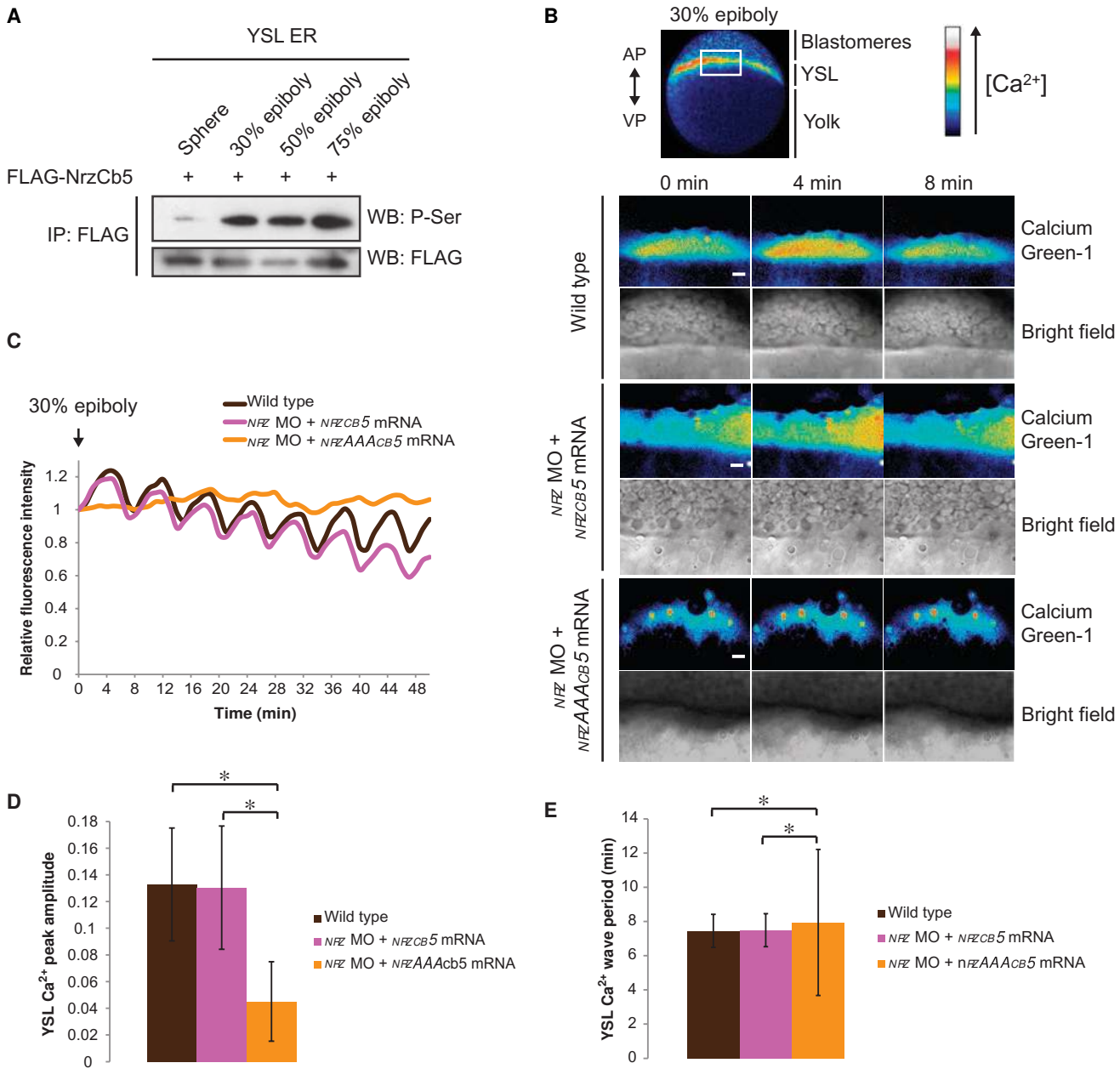

Fig. 7. Nrz phosphorylation is required for generation of cyclic Ca^{2+} waves in the YSL. (**A**) Representative Western blot of IP for FLAG-NrzCb5 from ER of YSL cells isolated from embryos at the indicated stages. $n = 3$. (**B**) Ca^{2+} concentration ($[Ca^{2+}]$) in the external YSL of uninjected wild-type embryos or embryos injected with *nrz* MO and *nrzcb5* or *nrzAAAcb5* mRNAs. Scale bars, 20 μm. (**C**) Representative graph of the $[Ca^{2+}]$ variation shown in (B). (**D** and **E**) Histograms showing the amplitude (D) or period (E) (mean ± SD) of YSL $[Ca^{2+}]$ as in (C). *$P < 0.005$ (Mann-Whitney *U* test). $n \geq 6$ embryos per condition.

concentration, and inhibition of IICR by Nrz did not require interaction with Bax. Moreover, phosphomimetic mutations in Nrz prevented interaction with the IP_3BD of IP_3R1, suggesting that Nrz acts directly on IP_3R1-dependent Ca^{2+} release in a manner that depends on Nrz phosphorylation.

We found that Nrz was phosphorylated during early zebrafish epiboly, a process that requires Ca^{2+} signaling (*28*), and expression of Nrz with nonphosphorylatable amino acids suppressed cyclic Ca^{2+} waves at the beginning of epiboly, compromised actin-myosin ring formation at the blastoderm margin, and delayed or disrupted epiboly. Ca^{2+} waves begin at the time when the actin-myosin ring is formed (*12*, *28*), and our data are consistent with the fact that Nrz must be inhibited to enable this process. We observed that the period of Ca^{2+} waves in the YSL was about 7 min. During myofibrillogenesis, actin-myosin network assembly is regulated by Ca^{2+} transients with a similar period (*34*, *35*). At the blastoderm margin, actin associates with phospho–myosin-II (*36*). We previously demonstrated that increased cytosolic Ca^{2+} concentrations in embryos injected with *nrz* MO promotes MLC phosphorylation, which leads to premature actin-myosin ring formation at 30% epiboly (*14*). Thus, Ca^{2+}

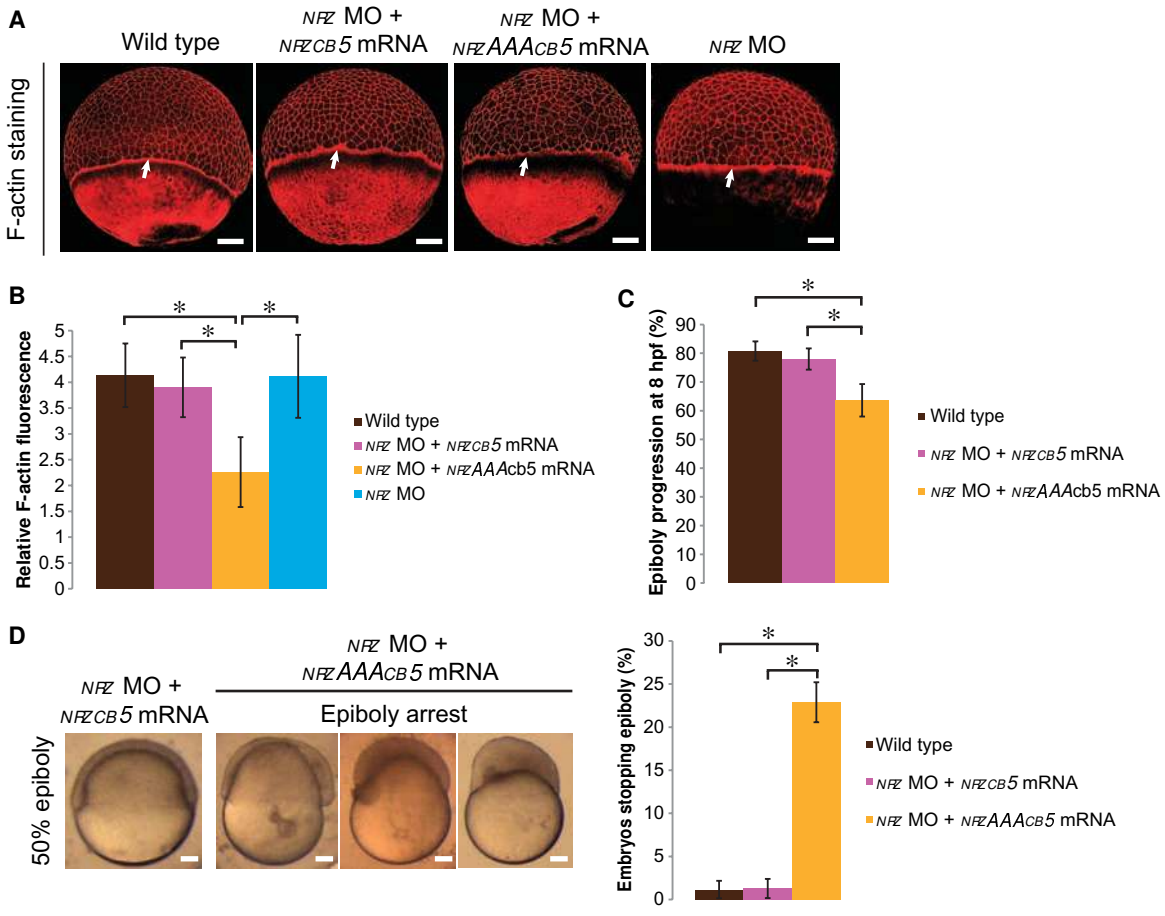

Fig. 8. Nrz phosphorylation is required for epiboly progression and actin ring formation. (**A**) Phalloidin-rhodamine staining of F-actin in embryos at the shield stage injected with *nrz* MO alone or in combination with *nrzcb5* or *nrzAAAcb5* mRNA. White arrows indicate the actin-myosin ring. (**B**) Histogram showing the relative actin fluorescence (mean ± SD). Relative fluorescence is indicative of the amount of F-actin at the blastoderm margin and was calculated by using the ratio of the rhodamine fluorescence at the blastoderm margin to the rhodamine fluorescence in the blastomeres. n = 30 embryos per condition. (**C**) Histogram showing the mean percentage (±SD) of epiboly progression at 8 hours post-fertilization (hpf). n = 90 embryos from 3 independent injections. (**D**) Representative images of the phenotypes (epiboly arrest) of embryos at 5 hpf injected with *nrz* MO and *nrzcb5* or *nrzAAAcb5* mRNA. NrzCb5 restores epiboly progression (50% epiboly), in contrast to NrzAAACb5 (epiboly arrest). n = 3 independent injections (80 to 100 embryos per injection per condition). Scale bars, 20 μm. *P < 0.005 (Mann-Whitney U test) for (B) to (D).

waves during early epiboly could time MLC phosphorylation and the progressive assembly of the actin-myosin ring.

Our results identify the role of Nrz in IICR and emphasize the role of Bcl-2 family proteins in the regulation of intracellular Ca^{2+}. We recently demonstrated that Bcl-wav, a newly characterized Bcl-2 family member, is essential for convergence and extension movement in zebrafish gastrulation. During this process, Bcl-wav regulates the formation of actin protrusions via its role in mitochondrial Ca^{2+} uptake (*37*). Together, these studies emphasize the diversity of functional roles of Bcl-2 family proteins in numerous cellular processes.

MATERIALS AND METHODS

MOs, reagents, and antibodies

The *nrz* MO was designed according to the manufacturer's recommendations (Gene Tools, LLC) and had the following sequence: 5′-CATTTTCCTCCCAGCGATGTCAGAC-3′. A second MO that contained four mismatches relative to *nrz* MO was used as a negative control (control MO). The sequence was as follows: 5′-CATTATCCTGCCAGCCATGTGAGAC-3′ (*13*).

The following antibodies were used: IP_3R1 (PA1-901, Thermo Scientific), rabbit FLAG (F-7425, Sigma-Aldrich), mouse FLAG (F-3165, Sigma-Aldrich), rabbit hemagglutinin (HA) (Ab75640, Abcam), mouse HA (MMS-101P, Covance), PARP (Ab6079, Abcam), vinculin (SC-55465, Santa Cruz Biotechnology), Bax (5023, Cell Signaling), and phosphoserine (05-1000, Millipore).

Vector construction and mRNA in vitro transcription

The open reading frames of *nrz* and *zbax* were cloned into the pCS2+ expression vector as previously described (*13*). The transmembrane domain of Cb5 was cloned in pCS2+ as previously described (*14*). Mutants of Nrz were inserted between the Cla I and Xho I restriction sites in the pCS2+Cb5 or pCS2+ vectors. For cloning of *zip$_3$r1*, total RNA from

embryos was extracted using TRIzol reagent (Invitrogen) following the manufacturer's instructions, and complementary DNA (cDNA) was generated with a cDNA synthesis kit (iScript cDNA synthesis kit, Bio-Rad) with 500 ng of total RNA and gene-specific primers. An HA tag was added to the N terminus by polymerase chain reaction. Gene fragments corresponding to the IP_3R1 domains were amplified and cloned between the Cla I and Xho I or between the Eco RI and Xho I sites in pCS2+. pcDNA3.1-IRIS was provided by K. Mikoshiba (*25*). In vitro transcription for the different constructs was performed with the SP6 mMESSAGE mMACHINE kit according to the manufacturer's recommendations (Ambion).

Zebrafish husbandry, manipulation, injection, and analysis

Zebrafish (crosses between AB and TU or between AB and TL strains) were raised and maintained according to standard procedures (*38*). Zebrafish embryos were grown in E3 medium (5 mM NaCl, 0.17 mM KCl, 0.33 mM $CaCl_2$, 0.33 mM $MgSO_4$, pH 7.6) at 28.5°C.

MO (0.5 mM) and mRNA (100 ng/ml) injections were performed between the one- and four-cell stages. Embryos were then observed every 15 min, and embryos showing margin constriction and cell detachment from the yolk were recorded as "embryos with a phenotype." Calcium Green-1 Dextran (Invitrogen) at 250 μM was injected at the 128-cell stage into the top of the yolk, close to the margin of the yolk and blastoderm.

Images of embryos at 8 hpf were acquired with a Nikon TE30 inverted microscope and MetaMorph software. Epiboly was quantified with Image J software by measuring the distance of the blastoderm margin from the animal pole (*D*) and the size of the embryos (*S*). Epiboly progression data were obtained by using the ratio *D*/*S*. F-actin staining of embryos was performed as previously described (*36*). In brief, embryos at the desired stage were fixed overnight in 4% paraformaldehyde at 4°C and washed in PBT [0.1% Triton-X 100 in phosphate-buffered saline (PBS)]. They were then permeabilized for 1 hour in 0.5% Triton-X in PBS and subsequently incubated in block solution (10% goat serum, 1% dimethyl sulfoxide, 0.1% Triton-X 100 in PBS) for 5 hours. The embryos were then incubated in rhodamine-phalloidin (Invitrogen) overnight at 4°C and washed three times in PBT.

Embryos used for Ca^{2+} imaging were injected with Calcium Green-1 Dextran (Invitrogen) at 250 μM into the top of the yolk at the blastoderm margin of 128-cell stage embryos (*10*), dechorionated, and mounted in low–melting point 0.7% agarose in E3 medium on the stage of a Zeiss LSM 780 microscope and incubated at 28.5°C. Stacks of 4 μm were acquired, and the sum of the first three stacks was used to visualize variations in Ca^{2+} concentration in the external YSL.

ER from the YSL was isolated as described previously (*14*). The 100,000*g* pellet was resuspended in TNE buffer [10 mM tris-HCl, 200 mM NaCl, 1 mM EDTA (pH 7.4), 1 mM β-glycerophosphate, 1 mM orthovanadate, 0.1 mM sodium pyrophosphate containing protease inhibitors] and was used for FLAG immunoprecipitation.

Cell culture, immunoprecipitation, Ca^{2+} imaging, and FRET

HeLa cells were grown in Dulbecco's modified Eagle's medium (high glucose) (Gibco) supplemented with 10% fetal bovine serum and 1% penicillin-streptomycin (Gibco) at 37°C in a 5% CO_2 humidified atmosphere.

For endogenous IP_3R and Bax coimmunoprecipitation experiments, 6×10^6 HeLa cells were transfected with the indicated vectors. After 24 hours, cells were lysed in TNE buffer. Extracts were precleared with protein G–Sepharose beads for 1 hour at 4°C and then incubated overnight with 5 μg of IP_3R or Bax primary antibody. The extracts were then incubated with protein G–Sepharose beads for 2 hours. Immunoprecipitated fractions were washed three times with TNE and analyzed by immunoblotting. For HA and FLAG immunoprecipitation, 1×10^6 HeLa cells were transfected with the indicated vectors and lysed and processed as above. One microgram of primary rabbit HA or rabbit FLAG was used.

For Ca^{2+} imaging, HeLa cells cultured in Nunc Lab-Tek chambered cover glass were incubated with 5 μM FluoForte (Enzo Life Sciences) in a Ca^{2+}-free balanced salt solution (BSS) [121 mM NaCl, 5.4 mM KCl, 0.8 mM $MgCl_2$, 6 mM $NaHCO_3$, 5.5 mM D-glucose, 25 mM Hepes (pH 7.3)] for 1 hour at 37°C. Fluorescence values were collected using a Zeiss LSM 780 confocal microscope. After 10 s of measurement, 5 μM histamine (Sigma) or thapsigargin (Enzo Life Sciences) in Ca^{2+}-free BSS was injected. For IRIS FRET, HeLa cells cultured in Nunc Lab-Tek chambered cover glass were cotransfected with pcDNA3.1-IRIS (*25*) and pCS2+ encoding the various Nrz mutants (n_{mole} ratio, 1:3). Before imaging, the medium was replaced with BSS. FRET was measured with a Zeiss LSM 780 confocal microscope by excitation at 405 nm. ECFP and Venus fluorescence were detected at 450 to 510 nm and 525 to 565 nm, respectively. After 10 s of measurement, 5 μM histamine in BSS was injected. Changes in the FRET signal were calculated using the F_{ECFP}/F_{Venus} ratio (*R*).

IP_3-FITC fluorescence polarization measurement

IP_3-FITC, IP_3, and the recombinant N-terminal domain protein were purchased with the HitHunter IP_3 assay kit from DiscoveRx. Recombinant Nrz protein was produced as previously described (*13*). IP_3-FITC at 0.5 nM was incubated with 4 nM of recombinant NTD and the various recombinant Nrz proteins for 30 min at 25°C. Fluorescence polarization was recorded at 25°C with 485-nm excitation and 530-nm emission filters, using a Mithras LB 940 multimode microplate reader (Berthold Technologies).

Sequence alignment

Nrz ortholog sequences were found in the National Center for Biotechnology Information protein database. Sequence alignment was performed with the Clustal Omega tool at http://www.ebi.ac.uk/Tools/msa/clustalo/. An image of the alignment was obtained with Jalview software (*39*).

Molecular docking simulation

The Nrz protein structure was obtained by analyzing the Nrz amino acid sequence on the Phyre^2 (*40*) homology modeling server. The Nrz BH4 domain structure was extracted, and a docking experiment was performed against the IP_3R1 binding domain crystal structure (PDB: 1N4K) using the PatchDock server (*41*). Images were acquired with UCSF Chimera software (*42*).

Statistical analysis

Statistical significance was analyzed using the Mann-Whitney *U* test; $P < 0.005$ was considered significant.

SUPPLEMENTARY MATERIALS

www.sciencesignaling.org/cgi/content/full/7/312/ra14/DC1

List of primers

Fig. S1. Sequence alignment of the BH4 domains of Nrz, zBcl-2, and zBcl-xL.

Fig. S2. Interaction of Nrz with IP_3BD requires the BH4 domain.

Fig. S3. Sequence alignment of the BH4 domains of Nrz orthologs.

Fig. S4. Nrz does not reduce the ER Ca^{2+} content.

Movie S1. Ca^{2+} waves in the YSL of a wild-type uninjected embryo.

Movie S2. Ca^{2+} waves in the YSL of an *nrzcb5*-injected embryo.

Movie S3. Ca^{2+} waves in the YSL of an *nrzAAAcb5*-injected embryo.

REFERENCES AND NOTES

1. R. J. Youle, A. Strasser, The BCL-2 protein family: Opposing activities that mediate cell death. *Nat. Rev. Mol. Cell Biol.* **9**, 47–59 (2008).
2. B. Bonneau, J. Prudent, N. Popgeorgiev, G. Gillet, Non-apoptotic roles of Bcl-2 family: The calcium connection. *Biochim. Biophys. Acta* **1833**, 1755–1765 (2013).
3. K. Uchida, H. Miyauchi, T. Furuichi, T. Michikawa, K. Mikoshiba, Critical regions for activation gating of the inositol 1,4,5-trisphosphate receptor. *J. Biol. Chem.* **278**, 16551–16560 (2003).
4. I. Bosanac, T. Michikawa, K. Mikoshiba, M. Ikura, Structural insights into the regulatory mechanism of IP_3 receptor. *Biochim. Biophys. Acta* **1742**, 89–102 (2004).
5. Y. P. Rong, A. S. Aromolaran, G. Bultynck, F. Zhong, X. Li, K. McColl, S. Matsuyama, S. Herlitze, H. L. Roderick, M. D. Bootman, G. A. Mignery, J. B. Parys, H. De Smedt, C. W. Distelhorst, Targeting Bcl-2-IP_3 receptor interaction to reverse Bcl-2's inhibition of apoptotic calcium signals. *Mol. Cell* **31**, 255–265 (2008).
6. C. White, C. Li, J. Yang, N. B. Petrenko, M. Madesh, C. B. Thompson, J. K. Foskett, The endoplasmic reticulum gateway to apoptosis by Bcl-X_L modulation of the $InsP_3R$. *Nat. Cell Biol.* **7**, 1021–1028 (2005).
7. M. J. Berridge, P. Lipp, M. D. Bootman, The versatility and universality of calcium signalling. *Nat. Rev. Mol. Cell Biol.* **1**, 11–21 (2000).
8. O. Markova, P. F. Lenne, Calcium signaling in developing embryos: Focus on the regulation of cell shape changes and collective movements. *Semin. Cell Dev. Biol.* **23**, 298–307 (2012).
9. C. B. Kimmel, W. W. Ballard, S. R. Kimmel, B. Ullmann, T. F. Schilling, Stages of embryonic development of the zebrafish. *Dev. Dyn.* **203**, 253–310 (1995).
10. M. Y. F. Yuen, S. E. Webb, C. M. Chan, B. Thisse, C. Thisse, A. L. Miller, Characterization of Ca^{2+} signaling in the external yolk syncytial layer during the late blastula and early gastrula periods of zebrafish development. *Biochim. Biophys. Acta* **1833**, 1641–1656 (2013).
11. S. E. Webb, A. L. Miller, Calcium signalling during embryonic development. *Nat. Rev. Mol. Cell Biol.* **4**, 539–551 (2003).
12. M. Behrndt, G. Salbreux, P. Campinho, R. Hauschild, F. Oswald, J. Roensch, S. W. Grill, C. P. Heisenberg, Forces driving epithelial spreading in zebrafish gastrulation. *Science* **338**, 257–260 (2012).
13. E. Arnaud, K. F. Ferri, J. Thibaut, Z. Haftek-Terreau, A. Aouacheria, D. Le Guellec, T. Lorca, G. Gillet, The zebrafish bcl-2 homologue Nrz controls development during somitogenesis and gastrulation via apoptosis-dependent and -independent mechanisms. *Cell Death Differ.* **13**, 1128–1137 (2006).
14. N. Popgeorgiev, B. Bonneau, K. F. Ferri, J. Prudent, J. Thibaut, G. Gillet, The apoptotic regulator Nrz controls cytoskeletal dynamics via the regulation of Ca^{2+} trafficking in the zebrafish blastula. *Dev. Cell* **20**, 663–676 (2011).
15. Y. P. Rong, G. Bultynck, A. S. Aromolaran, F. Zhong, J. B. Parys, H. De Smedt, G. A. Mignery, H. L. Roderick, M. D. Bootman, C. W. Distelhorst, The BH4 domain of Bcl-2 inhibits ER calcium release and apoptosis by binding the regulatory and coupling domain of the IP3 receptor. *Proc. Natl. Acad. Sci. U.S.A.* **106**, 14397–14402 (2009).
16. G. Monaco, E. Decrock, H. Akl, R. Ponsaerts, T. Vervliet, T. Luyten, M. De Maeyer, L. Missiaen, C. W. Distelhorst, H. De Smedt, J. B. Parys, L. Leybaert, G. Bultynck, Selective regulation of IP_3-receptor-mediated Ca^{2+} signaling and apoptosis by the BH4 domain of Bcl-2 versus Bcl-Xl. *Cell Death Differ.* **19**, 295–309 (2012).
17. T. A. Brock, E. A. Capasso, Thrombin and histamine activate phospholipase C in human endothelial cells via a phorbol ester-sensitive pathway. *J. Cell. Physiol.* **136**, 54–62 (1988).
18. X. M. Yin, Z. N. Oltvai, S. J. Korsmeyer, BH1 and BH2 domains of Bcl-2 are required for inhibition of apoptosis and heterodimerization with Bax. *Nature* **369**, 321–323 (1994).
19. E. F. Eckenrode, J. Yang, G. V. Velmurugan, J. K. Foskett, C. White, Apoptosis protection by Mcl-1 and Bcl-2 modulation of inositol 1,4,5-trisphosphate receptor-dependent Ca^{2+} signaling. *J. Biol. Chem.* **285**, 13678–13684 (2010).
20. G. Monaco, M. Beckers, H. Ivanova, L. Missiaen, J. B. Parys, H. De Smedt, G. Bultynck, Profiling of the Bcl-2/Bcl-X_L-binding sites on type 1 IP_3 receptor. *Biochem. Biophys. Res. Commun.* **428**, 31–35 (2012).
21. I. Bosanac, J. R. Alattia, T. K. Mal, J. Chan, S. Talarico, F. K. Tong, K. I. Tong, F. Yoshikawa, T. Furuichi, M. Iwai, T. Michikawa, K. Mikoshiba, M. Ikura, Structure of the inositol 1,4,5-trisphosphate receptor binding core in complex with its ligand. *Nature* **420**, 3–7 (2002).
22. H. Ando, A. Mizutani, T. Matsu-ura, K. Mikoshiba, IRBIT, a novel inositol 1,4,5-trisphosphate (IP_3) receptor-binding protein, is released from the IP_3 receptor upon IP_3 binding to the receptor. *J. Biol. Chem.* **278**, 10602–10612 (2003).
23. H. Ando, A. Mizutani, H. Kiefer, D. Tsuzurugi, T. Michikawa, K. Mikoshiba, IRBIT suppresses IP_3 receptor activity by competing with IP_3 for the common binding site on the IP_3 receptor. *Mol. Cell* **22**, 795–806 (2006).
24. C. J. Hanson, M. D. Bootman, C. W. Distelhorst, R. J. H. Wojcikiewicz, H. L. Roderick, Bcl-2 suppresses Ca^{2+} release through inositol 1,4,5-trisphosphate receptors and inhibits Ca^{2+} uptake by mitochondria without affecting ER calcium store content. *Cell Calcium* **44**, 324–338 (2008).
25. T. Matsu-ura, T. Michikawa, T. Inoue, A. Miyawaki, M. Yoshida, K. Mikoshiba, Cytosolic inositol 1,4,5-trisphosphate dynamics during intracellular calcium oscillations in living cells. *J. Cell Biol.* **173**, 755–765 (2006).
26. A. M. Rossi, C. W. Taylor, Analysis of protein-ligand interactions by fluorescence polarization. *Nat. Protoc.* **6**, 365–387 (2011).
27. M. C. Bassik, L. Scorrano, S. A. Oakes, T. Pozzan, S. J. Korsmeyer, Phosphorylation of BCL-2 regulates ER Ca^{2+} homeostasis and apoptosis. *EMBO J.* **23**, 1207–1216 (2004).
28. J. C. Cheng, A. L. Miller, S. E. Webb, Organization and function of microfilaments during late epiboly in zebrafish embryos. *Dev. Dyn.* **231**, 313–323 (2004).
29. J. M. Vicencio, C. Ortiz, A. Criollo, A. W. Jones, O. Kepp, L. Galluzzi, N. Joza, I. Vitale, E. Morselli, M. Tailler, M. Castedo, M. C. Maiuri, J. Molgó, G. Szabadkai, S. Lavandero, G. Kroemer, The inositol 1,4,5-trisphosphate receptor regulates autophagy through its interaction with Beclin 1. *Cell Death Differ.* **16**, 1006–1017 (2009).
30. S. Zhang, S. Malmersjö, J. Li, H. Ando, O. Aizman, P. Uhlén, K. Mikoshiba, A. Aperia, Distinct role of the N-terminal tail of the Na,K-ATPase catalytic subunit as a signal transducer. *J. Biol. Chem.* **281**, 21954–21962 (2006).
31. A. Miyakawa-Naito, P. Uhlén, M. Lal, O. Aizman, K. Mikoshiba, H. Brismar, S. Zelenin, A. Aperia, Cell signaling microdomain with Na,K-ATPase and inositol 1,4,5-trisphosphate receptor generates calcium oscillations. *J. Biol. Chem.* **278**, 50355–50361 (2003).
32. J. Hirota, H. Ando, K. Hamada, K. Mikoshiba, Carbonic anhydrase-related protein is a novel binding protein for inositol 1,4,5-trisphosphate receptor type 1. *Biochem. J.* **372**, 435–441 (2003).
33. L. Scorrano, S. A. Oakes, J. T. Opferman, E. H. Cheng, M. D. Sorcinelli, T. Pozzan, S. J. Korsmeyer, BAX and BAK regulation of endoplasmic reticulum Ca^{2+}: A control point for apoptosis. *Science* **300**, 135–139 (2003).
34. M. B. Ferrari, J. Rohrbough, N. C. Spitzer, Spontaneous calcium transients regulate myofibrillogenesis in embryonic *Xenopus* myocytes. *Dev. Biol.* **178**, 484–497 (1996).
35. H. Li, J. D. Cook, M. Terry, N. C. Spitzer, M. B. Ferrari, Calcium transients regulate patterned actin assembly during myofibrillogenesis. *Dev. Dyn.* **229**, 231–242 (2004).
36. M. Köppen, B. G. Fernández, L. Carvalho, A. Jacinto, C. P. Heisenberg, Coordinated cell-shape changes control epithelial movement in zebrafish and *Drosophila*. *Development* **133**, 2671–2681 (2006).
37. J. Prudent, N. Popgeorgiev, B. Bonneau, J. Thibaut, R. Gadet, J. Lopez, P. Gonzalo, R. Rimokh, S. Manon, C. Houart, P. Herbomel, A. Aouacheria, G. Gillet, Bcl-wav and the mitochondrial calcium uniporter drive gastrula morphogenesis in zebrafish. *Nat. Commun.* **4**, 2330 (2013).
38. M. Westerfield, *A Guide for the Laboratory Use of Zebrafish (Danio rerio)* (University of Oregon Press, Eugene, OR, ed. 3, 1995).
39. A. M. Waterhouse, J. B. Procter, D. M. A. Martin, M. Clamp, G. J. Barton, Jalview Version 2—A multiple sequence alignment editor and analysis workbench. *Bioinformatics* **25**, 1189–1191 (2009).
40. L. A. Kelley, M. J. E. Sternberg, Protein structure prediction on the Web: A case study using the Phyre server. *Nat. Protoc.* **4**, 363–371 (2009).
41. D. Schneidman-Duhovny, Y. Inbar, R. Nussinov, H. J. Wolfson, PatchDock and SymmDock: Servers for rigid and symmetric docking. *Nucleic Acids Res.* **33**, W363–W367 (2005).
42. E. F. Pettersen, T. D. Goddard, C. C. Huang, G. S. Couch, D. M. Greenblatt, E. C. Meng, T. E. Ferrin, UCSF Chimera—A visualization system for exploratory research and analysis. *J. Comput. Chem.* **25**, 1605–1612 (2004).

Acknowledgments: We thank K. Mikoshiba for providing the IRIS construct and S. Chabaud (UBET, Centre Léon Bérard), C. Vanbelle (CeCILE—SFR Santé Lyon-Est), and C. Bouchardon (CeCILE—SFR Santé Lyon-Est) for their technical assistance. **Funding:** This work was supported by AFMTéléthon, Ligue nationale contre le cancer (comité de la Drôme), Fondation ARC pour la recherche sur le cancer. B.B. and A.N. are fellows of the Ministère de la Recherche. N. Peyriéras received support from France BioImaging ANR-10-INBS-04 (BioEmergences platform). **Author contributions:** B.B., A.N., J.P., and N. Popgeorgiev performed the experiments. B.B., N. Peyriéras, R.R., and G.G. designed the experiments. B.B. and G.G. wrote the manuscript. **Competing interests:** The authors declare that they have no competing interests.